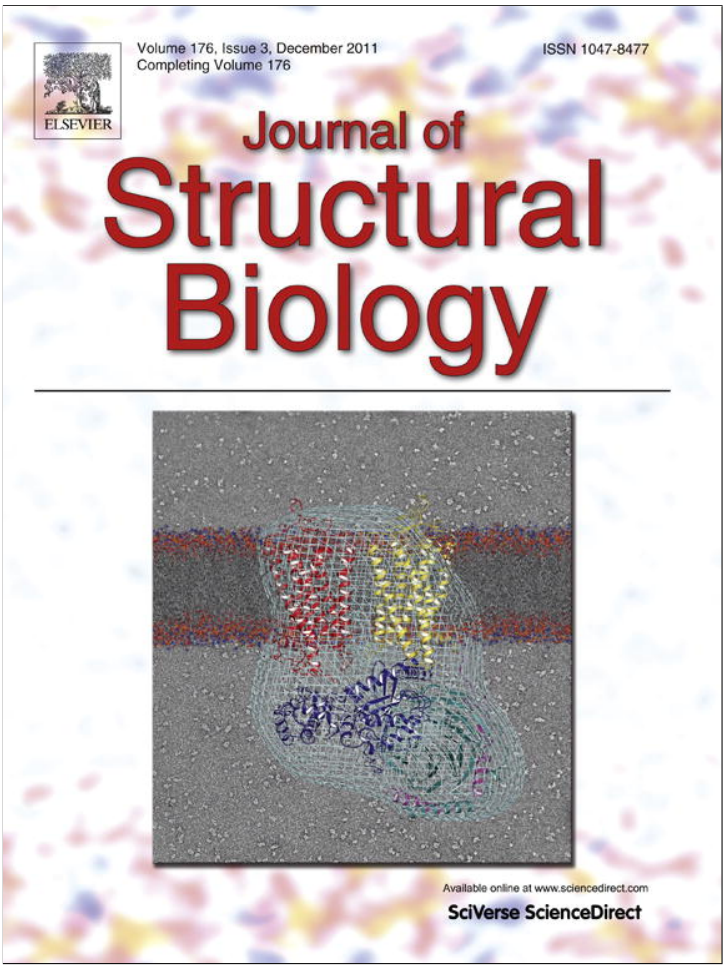

Journal of Structural Biology 176 (2011) 279–291

Contents lists available at SciVerse ScienceDirect

Journal of Structural Biology

journal homepage: www.elsevier.com/locate/yjsbi

Structural and functional insights into a dodecameric molecular machine – The RuvBL1/RuvBL2 complex

Sabine Gorynia [a,b,1], Tiago M. Bandeiras [c], Filipa G. Pinho [c], Colin E. McVey [a], Clemens Vonrhein [d], Adam Round [e,2], Dmitri I. Svergun [e], Peter Donner [a,b], Pedro M. Matias [a], Maria Arménia Carrondo [a,*]

[a] Instituto de Tecnologia Química e Biológica, Universidade Nova de Lisboa, Apartado 127, 2781-901 Oeiras, Portugal
[b] Bayer Schering Pharma AG, Lead Discovery Berlin – Protein Supply, 13353 Berlin, Germany
[c] Instituto de Biologia Experimental e Tecnológica, Apartado 12, 2781-901 Oeiras, Portugal
[d] Global Phasing Ltd., Sheraton House, Castle Park, Cambridge CB3 0AX, UK
[e] European Molecular Biology Laboratory, Hamburg Outstation, Notkestrasse 85, 22603 Hamburg, Germany

ARTICLE INFO

Article history:
Received 23 March 2011
Received in revised form 12 August 2011
Accepted 2 September 2011
Available online 10 September 2011

Keywords:
AAA$^+$ proteins
Chromatin remodeling
Helicase
X-ray crystallography

An interactive 3D complement page in Proteopedia is available at: http://proteopedia.org/w/Journal:JSB:1

ABSTRACT

RuvBL1 (RuvB-like 1) and its homolog RuvBL2 are evolutionarily highly conserved AAA$^+$ ATPases essential for many cellular activities. They play an important role in chromatin remodeling, transcriptional regulation and DNA damage repair. RuvBL1 and RuvBL2 are overexpressed in different types of cancer and interact with major oncogenic factors, such as β-catenin and c-Myc regulating their function. We solved the first three-dimensional crystal structure of the human RuvBL complex with a truncated domain II and show that this complex is competent for helicase activity. The structure reveals a dodecamer consisting of two heterohexameric rings with alternating RuvBL1 and RuvBL2 monomers bound to ADP/ATP, that interact with each other via the retained part of domain II. The dodecameric quaternary structure of the R1ΔDII/R2ΔDII complex observed in the crystal structure was confirmed by small-angle X-ray scattering analysis.

Interestingly, truncation of domain II led to a substantial increase in ATP consumption of RuvBL1, RuvBL2 and their complex. In addition, we present evidence that DNA unwinding of the human RuvBL proteins can be auto-inhibited by domain II, which is not present in the homologous bacterial helicase RuvB. Our data give new insights into the molecular arrangement of RuvBL1 and RuvBL2 and strongly suggest that *in vivo* activities of these highly interesting therapeutic drug targets are regulated by cofactors inducing conformational changes via domain II in order to modulate the enzyme complex into its active state.

1. Introduction

RuvBL1 and RuvBL2 are implicated in many cellular pathways (Jha and Dutta, 2009) and function predominantly as part of chromatin remodeling complexes. Most chromatin remodeling complexes are typically considered to be transcriptional regulators, but different roles have recently been assigned beyond transcription, such as cell cycle checkpoint activation, DNA repair and replication, telomere regulation, centromere stability and chromosome segregation (Morrison and Shen, 2009). The assumption that these complexes play a key role in many essential cellular processes beyond transcription, suggests the existence of a sophisticated regulatory system modulating the chromatin remodeling activity of each complex for each different role. How these regulatory mechanisms modulate such functional diversity has been a puzzling feature of chromatin remodeling.

RuvBL1 and RuvBL2 are part of various ATP-dependent chromatin remodeling complexes, such as INO80, SWR1, p400 and TIP60 (Ikura et al., 2000; Jonsson et al., 2001, 2004; Kusch et al., 2004; Mizuguchi et al., 2004; Samuelson et al., 2005; Shen et al., 2000). These ubiquitously expressed proteins (Bauer et al., 1998) belong to the AAA$^+$ family of ATPases (ATPases associated with diverse

Abbreviations: ADP, adenosine diphosphate; ATP, adenosine triphosphate; BSA, bovine serum albumin; dsDNA, double-stranded Deoxyribonucleic acid; ssDNA, single-stranded Deoxyribonucleic acid; HEPES, 4-(2-hydroxyethyl)-1-piperazineethanesulfonic acid; MAD, multi-wavelength anomalous dispersion; NCS, non-crystallographic symmetry; PEG, polyethylene glycol; R1ΔDII, RuvBL1 with truncated domain II; R2ΔDII, RuvBL2 with truncated domain II; SAXS, small-angle X-ray scattering; SeMet, selenomethionine; SSM, secondary structure matching; SV40 Ltag, Simian Virus 40 large tumor antigen; TCEP, tris(2-carboxyethyl)phosphine; Tris, tris(hydroxymethyl)aminomethane.

* Corresponding author. Fax: +351 21 4433644.
E-mail address: carrondo@itqb.unl.pt (M.A. Carrondo).
[1] Current address: UCLA, Department of Biological Chemistry, David Geffen School of Medicine, 615 Charles E. Young Drive South, Box 951737, BSRB#390C, Los Angeles, CA 90095-1737, United States.
[2] Current address: European Molecular Biology Laboratory, Grenoble Outstation, 6 Rue Jules Horowitz, 38042 Grenoble Cedex 9, France.

1047-8477/$ - see front matter © 2011 Elsevier Inc. All rights reserved.
doi:10.1016/j.jsb.2011.09.001

cellular activities) (Neuwald et al., 1999). This class of ATPases includes nucleic acid processing enzymes, chaperones and proteases that contain conserved motifs for ATP-binding and hydrolysis such as the Walker A and Walker B boxes (Walker et al., 1982), sensor residues and the Arg-finger. AAA^+ proteins use the hydrolysis of ATP to exert mechanical forces, and this has been shown to be essential for the biological activity of RuvBL1 and RuvBL2 (Feng et al., 2003; Jonsson et al., 2004; Wood et al., 2000). RuvBL1 and RuvBL2 share 43% sequence identity and 65% sequence similarity and are homologs of the bacterial DNA-dependent ATPase and helicase RuvB (Putnam et al., 2001; Yamada et al., 2001). However, the original data reporting DNA helicase activities of RuvBL1 (Makino et al., 1999) and RuvBL2 (Kanemaki et al., 1999) were not reproducible with the purified wild-type proteins (Ikura et al., 2000; Qiu et al., 1998). Although RuvBL1 and RuvBL2 share structural features with bacterial RuvB (Matias et al., 2006), domain II is not present in the bacterial homolog and had to be truncated in the RuvBL proteins used for structural analysis in this work.

A link between RuvBL1, RuvBL2 and cancer has been established in the last decade. Both proteins interact with transcription regulators known to be involved in oncogenic pathways, such as β-catenin and c-Myc. Among the transcription factors with oncogenic potential, c-Myc is one of the most frequent sites of mutation in human cancer (Cole, 1986), while β-catenin has a key role in Wnt signaling via effects on T-cell factor (TCF)-mediated transcription (Bauer et al., 1998, 2000; Feng et al., 2003).

It was shown that RuvBL1 is required for the transforming effect of c-Myc (Wood et al., 2000), the viral oncoprotein E1A (Dugan et al., 2002) and β-catenin (Feng et al., 2003). Studies from different groups report an overexpression of RuvBL1 and RuvBL2 in several types of cancer, such as bladder cancer, melanoma, non-small cell lung cancer, gastric cancer and colon cancer (Dehan et al., 2007; Lauscher et al., 2007; Rousseau et al., 2007). A differential proteomic analysis of human hepatocellular carcinoma revealed an overexpression of RuvBL1 and RuvBL2, and both proteins were considered markers of poor prognosis (Blanc et al., 2005; Huber et al., 2008). These findings imply that both proteins are not only of general interest for oncologists, but might also represent highly effective therapeutic drug targets.

To date there is no crystal structure available for the RuvBL1/RuvBL2 complex, but electron microscopy (EM) studies of the yeast and human complex show that RuvBL1 and RuvBL2 form a dodecameric complex consisting of two structurally distinct hexameric rings (Puri et al., 2007; Torreira et al., 2008). The yeast model suggests that domain II forms the interaction site between two hexameric rings (Torreira et al., 2008), but neither study settled the issues of whether the rings are homo- or hetero-oligomeric and if they interchange depending on different chromatin remodeling functions. Furthermore, Gribun and co-workers proposed from EM studies a single heterohexameric ring structure for the yeast RuvBL1/RuvBL2 complex (Gribun et al., 2008). The differences between the EM structures suggest that RuvBL1 and RuvBL2 may be capable of forming various complexes. Previous work showed that the weak ATPase activity of RuvBL1 and RuvBL2 *in vitro* increased synergistically when the proteins formed a double-hexameric complex demonstrating that this is the enzymatically active form (Ikura et al., 2000; Puri et al., 2007). A recent study analyzing the oligomeric assembly of the human RuvBL1/2 proteins suggests that the RuvBL1/RuvBL2 complex forms single and double hexamers together with smaller forms and that truncation of domain II destabilizes the dodecamer formation (Niewiarowski et al., 2010).

The need to clarify both the oligomerization-function relationships and the ATP hydrolysis mechanism, prompted us to perform further structural studies. To address these questions, the crystal structure of the human RuvBL1/RuvBL2 complex with bound ATP/ADP has been determined. Since the full-length complex did not crystallize, mutants of RuvBL1 (R1) and RuvBL2 (R2) with a two-thirds truncation of the flexible domain II (Matias et al., 2006) were generated (R1ΔDII and R2ΔDII). Crystals of the selenomethionine derivative of the R1ΔDII/R2ΔDII complex diffracted to 3 Å resolution and led to the determination of the three-dimensional structure of the complex. These structural data combined with functional studies provide a possible mode of *in vivo* activation of these highly conserved proteins.

2. Materials and methods

2.1. Protein purification

For biochemical studies, deletion mutants of RuvBL1 and RuvBL2 with truncations in their flexible domains II (Matias et al., 2006) were generated: R1ΔDII missing residues T127-E233 and R2ΔDII missing residues between E134-E237. A linker consisting of amino acids GPPG was inserted to replace the deleted region (see Supplementary Fig. S1). The RuvBL complexes were co-expressed in *Escherichia coli* BL21(DE3) using the pETDuet vector (Novagen) with RuvBL1 carrying a N-terminal 6xHis-tag and RuvBL2 a N-terminal FLAG-tag (details described in (Gorynia et al., 2008)). The selenomethionine derivative of the R1ΔDII/R2ΔDII complex was co-expressed in B834(DE3). All protein complexes were purified as previously described (Gorynia et al., 2008). The gel filtration peak was pooled and concentrated using an Amicon Ultra Centrifugal Filter with a 30 kDa cut-off to a final concentration of 12 mg/ml. A MALDI-TOF/TOF analysis showed that 9 out of 11 methionines in R1ΔDII and 10 out of 12 methionines in R2ΔDII were replaced by selenomethionines.

2.2. Crystallization of the RuvBL complex

Crystals of the SeMet R1ΔDII/R2ΔDII complex were obtained at 4 °C within 1 week by the sitting drop vapor diffusion technique. Crystallization drops were mixed from equal volumes of protein solution (12 mg/ml SeMet R1ΔDII/R2ΔDII, 20 mM Tris–HCl pH 8.0, 200 mM NaCl, 10% glycerol, 4 mM $MgCl_2$, 4 mM ADP, 0.5 mM TCEP) and crystallization solution (0.2 M $MgCl_2$, 22% PEG 400, 0.1 M HEPES pH 7.5). In order to optimize crystal quality and dimensions the reservoir precipitant concentration was increased up to 30% PEG 400. Within 1 week, fewer and larger crystals were observed with typical dimensions of 300 × 300 × 50 μm. No crystal growth occurred without co-crystallization with ADP, and attempts at co-crystallization with non-hydrolyzable ATP analogs were unsuccessful.

2.3. Structure determination

A 3-wavelength MAD data set was collected to a maximum resolution of 3 Å from a flash-cooled crystal of the SeMet R1ΔDII/R2ΔDII complex at beam line ID29 of the European Synchrotron Radiation Facility (ESRF) in Grenoble. The peak and inflection point energies were selected from a fluorescence scan near the absorption K-edge of selenium using CHOOCH (Evans and Pettifer, 2001) and the remote wavelength was chosen as 0.97633 Å. The crystal belonged to the orthorhombic space group $C222_1$ with unit cell parameters a = 111.8, b = 187.9, c = 244.9 Å and six monomers (three R1ΔDII and three R2ΔDII) in the asymmetric unit. For each wavelength, the data were first integrated and scaled with XDS (Kabsch, 1993), followed by merging with SCALA and converted to structure factors with CTRUNCATE in the CCP4 suite (Collaborative Computational Project Number 4, 1994). The data collection and processing statistics are presented in Table 1.

Table 1
Data collection and processing statistics.

	Peak	Inflection	Remote
Beamline		ESRF ID 29	
Detector		ADSC Quantum Q315r	
Wavelength (Å)	0.97930	0.97946	0.97633
Data processing		XDS	
Space group		$C222_1$	
Unit cell parameters (Å)	a = 111.7, b = 187.8, c = 245.0	a = 111.9, b = 188.2, c = 245.5	a = 111.8, b = 187.9, c = 244.9
Resolution (Å)	49.0–3.00 (3.16–3.00)	49.1–3.51 (3.70–3.51)	49.0–3.00 (3.16–3.00)
Nr. observations	445,261 (63,511)	278,292 (39,063)	220,177 (32,682)
Unique reflections	52,009 (7414)	32,762 (4653)	51,774 (7486)
Completeness (%)	99.8 (98.7)	99.8 (98.9)	99.7 (100.0)
R-merge (%)[a]	15.5 (168.5)	15.0 (94.6)	7.5 (76.4)
R-pim (%)[b]	6.6 (64.7)	6.0 (36.7)	5.3 (48.2)
R-meas (%)[c]	19.4 (190.9)	17.6 (107.1)	10.9 (100.5)
$\langle I/\sigma(I)\rangle$	10.9 (1.3)	12.4 (2.5)	12.0 (1.7)
Wilson plot B	96	–	95
Z[d]		3	
V_m		2.6	
Estimated solvent content (%)		53	

[a] R-merge = merging R-factor, $(\Sigma_{hkl}\,\Sigma_i\,|I_i(hkl) - \langle I(hkl)\rangle|)/(\Sigma_{hkl}\,\Sigma_i\,I(hkl)) \times 100\%$. In the MAD dataset, Bijvoet pairs were treated as separate observations during the scaling process.

[b] R-pim = precision independent R-factor, $\Sigma_{hkl}\,[1/(N_{hkl}-1)]^{1/2}\,\Sigma_i\,|I_i(hkl) - \langle I(hkl)\rangle|/\Sigma_{hkl}\,\Sigma_i\,I_i(hkl) \times 100\%$, where I is the observed intensity, $\langle I\rangle$ is the average intensity of multiple observations from symmetry-related reflections, and N_{hkl} is their multiplicity. (Diederichs and Karplus, 1997).

[c] R-meas = redundancy independent R-factor, $\Sigma_{hkl}\,[N_{hkl}/(N_{hkl}-1)]^{1/2}\,\Sigma_i\,|I_i(hkl) - \langle I(hkl)\rangle|/\Sigma_{hkl}\,\Sigma_i\,I_i(hkl) \times 100\%$. (Diederichs and Karplus, 1997).

[d] Nr. heterodimers in the asymmetric unit according to Matthews coefficient (Matthews, 1968).

The Se-atom substructure was determined by molecular replacement using PHASER (Storoni et al., 2004) with the homologous RuvBL1 monomer (Matias et al., 2006) as the search model, truncated to reflect the shortened domain II (Gorynia et al., 2008). The Se-atom positions were then located from an anomalous Fourier map. The strongest peaks in this map corresponded to the Se atom positions in the SeMet residues of the R1ΔDII and R2ΔDII monomers, allowing their identification in the crystal structure of the complex. A total of 51 selenium sites were located in this fashion, and input to a maximum-likelihood heavy-atom parameter refinement using autoSHARP (Vonrhein et al., 2007). The autoSHARP calculations found four additional sites. The centroid SHARP phases were further improved by density modification with DM (Cowtan, 1994) using non-crystallographic symmetry averaging (NCS). The NCS operator information was derived from the molecular replacement solution, assuming alternating R1ΔDII and R2ΔDII monomers. The results of the phasing calculations are summarized in Table 2. About 1800 residues of the expected 2235 could be built automatically with Buccaneer/REFMAC (Cowtan, 2006; Murshudov et al., 1997) and the molecular replacement solution was used to complete the model, together with the electron density maps obtained from the DM calculations. Protein chains A, B and C corresponded to the R1ΔDII monomers while chains D, E and F were assigned to the R2ΔDII monomers in the complex.

Table 2
Phase refinement statistics.

	Peak	Inflection	Remote	Overall
Phasing power, acentric	0.637	0.707	–	
Phasing power, centric	0.494	0.539	–	
Phasing power, anomalous	1.196	0.467	0.626	
Centric R_{cullis}	0.843	0.810	–	
Acentric R_{cullis}	0.857	0.819	–	
Anomalous R_{cullis}	0.772	0.931	0.916	
SHARP FOM, acentric				0.350
SHARP FOM, centric				0.307
Overall $\lvert E^2\rvert$ correlation[a]				0.759
FOM after final DM run[a]				0.830
FOM after NCS averaging[b]				0.759

[a] From the SHARP optimizing density modification procedure (SOLOMON (Abrahams and Leslie, 1996) followed by final DM (Cowtan, 1994) run).

[b] From the DM run using NCS.

2.4. Structure refinement

The crystal structure of the R1ΔDII/R2ΔDII complex was refined at 3 Å resolution against the remote data set with non-crystallographic symmetry restraints between equivalent monomers in the asymmetric unit and TLS (translation-libration-screw) rigid body refinement of atomic displacement parameters, followed by refinement of individual atomic parameters. For the initial refinement PHENIX was used (Adams et al., 2002) and gave R and R-free (Brünger, 1992) values of 0.202 and 0.229, respectively. The final refinement was carried out with BUSTER (Bricogne et al., 2010) using automatic non-crystallographic symmetry (NCS) restraint setup with pruning of significant outliers (Smart et al., 2008), TLS rigid body refinement and the so-called missing atom channel. For the latter, 3000 missing atoms were declared to be missing uniformly within the region not occupied by the current model. This model was refined to R and R-free values of 0.178 and 0.205. No water molecules were added. The model was periodically checked and corrected with COOT (Emsley and Cowtan, 2004) against $2|F_0| - |F_c|$ and $|F_0| - |F_c|$ electron-density maps. The R-free based estimate (Blow, 2002) of the overall coordinate error was 0.32 Å. The refinement statistics are presented in Table 3. The structure was analyzed with PROCHECK (Laskowski et al., 1993). Most stereochemical parameters were within their respective confidence intervals, while some non-glycine and non-proline residues were outside the most favored regions in a Ramachandran (Ramachandran and Sasisekharan, 1968) φ, ϕ plot (see Table 3). These outliers are located in regions with relatively poor electron density.

2.5. Small-angle X-ray scattering (SAXS) experiment and data analysis

The SAXS data were recorded at the EMBL beamline X33 on the DORIS storage ring at DESY in Hamburg (Roessle et al., 2007). A MAR345 image plate detector (MAR Research GmbH) was used at a sample-detector distance of 2.7 m covering the range of momentum transfer $0.012 < s < 0.45$ Å^{-1} ($s = 4\pi \sin\theta/\lambda$, where λ = 1.5 Å is the X-ray wavelength and 2θ is the scattering angle). No measurable radiation damage was detected by comparison of successive time frames with 2 min exposures. The corresponding buffer consisting of 20 mM Tris–HCl pH 8.0, 250 mM NaCl, 5% glycerol, 4 mM $MgCl_2$ and 2 mM β-mercaptoethanol, was measured

Table 3
Final refinement statistics.

Resolution limits (Å)					46.14–3.00 (3.08–3.00)	
R-factor (%)[a]					0.178 (0.247)	
Nr. reflections					49,101 (3580)	
Free R-factor (%)[b]					0.205 (0.270)	
Nr. reflections					2632 (219)	
Estimated coordinate error (Å)[c]					0.32	
Model composition						
Non-hydrogen protein atoms					14,473	
ATP					186	
Model r.m.s. deviations from ideality						
Bond lengths (Å)					0.009	
Bond angles (°)					1.1	
Model completeness and validation	Chain A	Chain B	Chain C	Chain D	Chain E	Chain F
Regions omitted	1–18	1–18	1–18	1–37	1–36	1–36
	139–145	138–145	140–144	147–154	147–154	147–154
	161–179	161–179	160–179	169–181	170–181	169–181
	363–367	365–367	364–367	369–378	372–378	369–378
Mean B values (Å^2)[d]						
Protein main-chain	102	113	107	108	110	100
Protein side-chain	113	124	118	118	121	112
ATP	88	103	95	99	97	89
Ramachandran plot statistics. Residues in						
Most favoured regions (%)	92.1	91.4	91.8	91.6	91.4	92.6
Allowed regions (%)	6.5	7.1	7.1	6.6	6.8	5.5
Generously allowed regions (%)	0.7	0.4	0.4	0.7	0.7	0.7
Disallowed regions (%)	0.7	1.1	0.7	1.1	1.1	1.1
PROCHECKG-factor	0.11	0.11	0.12	0.12	0.12	0.11

[a] R-factor = Σ_{hkl} $||F_o| - |F_c||/\Sigma_{hkl}$ $|F_o|$, where $|F_o|$ and $|F_c|$ are the observed and calculated structure factor amplitudes, respectively.

[b] Free R-factor is the cross-validation R-factor computed from a randomly chosen subset of 5% of the total number of reflections, which were not used during the refinement.

[c] Based on free R-factor (Blow, 2002).

[d] Calculated from equivalent isotropic *B* values, including the TLS contribution for the protein and ATP atoms.

before and after each protein sample. The samples were measured in the concentration range from 1 to 22 mg/ml; at least three different solute concentrations were measured for each construct. The data were analyzed following standard procedures using the programs from the ATSAS suite (Petoukhov et al., 2007). The radius of gyration R_g was evaluated using the Guinier approximation (Guinier, 1939) assuming that at very small angles ($s < 1.3/R_g$) the intensity is represented as $I(s) = I(0)\exp(-(sR_g)^{2/3})$, and from the entire scattering patterns using the indirect transform package GNOM (Svergun, 1992). The molecular mass (MM) of the solutes were estimated from the excluded particle volumes (Porod, 1982). For globular proteins, Porod (i.e. hydrated) volumes in Å^3 (taken from the *ab initio* shape models reconstructed as indicated below) are about 1.7–2 times the MMs in Da. All parameters calculated from scattering data were compared with the known (expected) values from other biochemical and structural techniques and checked for consistency to verify the monodispersity of the samples and the quality of the collected data. These data are included in Supplementary Table 1.

The *ab initio* low resolution structures were calculated using the program DAMMIN (Svergun, 1999). This program represents the particle shape by an assembly of densely packed beads and employs simulated annealing to construct a compact interconnected model fitting the experimental data $I_{exp}(s)$ to minimize discrepancy:

$$\chi^2 = \frac{1}{N-1}\sum_j \left[\frac{I_{exp}(S_j) - cI_{calc}(S_j)}{\sigma(S_j)}\right]^2, \quad (1)$$

where N is the number of experimental points, c is a scaling factor and $I_{calc}(s)$ and $\sigma(s_j)$ are the calculated intensity and the experimental error at the momentum transfer s_j, respectively.

To account for the flexible linkers in the dodecameric RuvBL1wt/RuvBL2ΔDII complex, BUNCH (Petoukhov and Svergun, 2005) was employed. The separate constituent domains of the monomer were taken as rigid bodies fixed to their positions in the crystal structure and the linkers were represented by chains of dummy residues. The BUNCH reconstructions were performed using the overall *P*32 symmetry of the dodecamer. To allow for possible asymmetry of the linkers, an alternative modeling was performed using CORAL (Petoukhov et al., in preparation), which is a new version of BUNCH allowing to work with multichain models and thus to add asymmetric fragments to symmetric structures. The scattering from the high resolution models of RuvBL1 monomers, hexameric and dodecameric rings for the RuvBL1/RuvBL2 constructs was computed by CRYSOL (Svergun et al., 1995) and these patterns were used to compute the fractions of double and single ring conformations using OLIGOMER (Konarev et al., 2003). The results are listed in Table 4.

2.6. Nucleic acid binding assay

A nucleotide oligomer (5′-CAGGCATGCAAGCTTGGCACTGGCC GTCGTTTTACAACGTCGTGACTGGGAAAACCCTGG-3′) was labeled with ^{33}P and used as ssDNA substrate. The binding reaction was performed in a final volume of 15 μl. SsDNA (1 pmol) was incubated with 10 pmol of purified protein in binding buffer (15 mM HEPES, pH 6.7, 10% glycerol, 1 mM EDTA, 500 μM ATP, 1 mM dithiothreitol, and 2 mM $MgCl_2$) for 30 min at room temperature. Hi-Density Tris borate EDTA (TBE) sample buffer (Invitrogen) was added to the reaction, and the sample was separated by a 6% PAGE with 0.5× TBE buffer and visualized by autoradiography. BSA was used as negative control.

2.7. ATPase assay

ATPase reactions were carried out as previously described (Matias et al., 2006). SV40 Ltag helicase was used as a positive control. The D302N mutant of RuvBL1 and the D299N mutant of RuvBL2 were used as negative controls. Molecular masses of 50 kDa (RuvBL1 and RuvBL2) and 90 kDa (SV40) were used to calculate moles of hydrolyzed ATP per mole of protein.

2.8. DNA helicase assay

A dsDNA substrate was generated to test helicase activities. To this effect, the ssDNA plasmid M13mp18 (New England Biolabs) was annealed with a complementary oligonucleotide (5′-AGTCACGACGTTGTA-3′) in hybridization buffer (10 mM Tris–HCl pH 7.5, 800 mM NaCl, 5 mM $MgCl_2$). The M13mp18 substrate was labeled with the Klenow Enzyme (Roche) using [α-^{33}P]-ATP in Klenow buffer (50 mM Tris–HCl pH 7.5, 10 mM $MgCl_2$, 1 mM DTT, 100 μg/ml BSA) at room temperature overnight and then purified from free nucleotides using the NucTrap® Probe Purification Columns (Stratagene). The DNA helicase assay was performed as previously described (Matias et al., 2006) using a protein concentration of 0.03 mg/ml. SV40 Ltag helicase was used as a positive control.

2.9. PDB accession codes

Atomic coordinates and structure factors have been deposited in the Protein Data Bank (Berman et al., 2000) with accession codes 2xsz and r2xszsf.

3. Results

3.1. Overall dodecameric structure of the RuvBL1ΔDII/RuvBL2ΔDII complex

The crystal structure of the R1ΔDII/R2ΔDII complex consists of dodecamers formed by two heterohexamers stacked on top of each

Table 4
Volume fractions of monomers, hexamers and dodecamers in solutions of RuvBL1, RuvBL2 and their complexes.

Sample	Monomer (%)	Hexamer (%)	Dodecamer (%)	χ
RuvBL1wt (<6 mg/mL)	97	3	0	2.9
RuvBL1wt (>6 mg/mL)	0	100	0	1.6
RuvBL2wt	0	82	18	5.4
RuvBL2ΔDII	0	77	23	1.4
RuvBL1wt/RuvBL2wt	0	54	46	2.9
RuvBL1wt/RuvBL2ΔDII	0	0	100	1.5
RuvBL1ΔDII/RuvBL2ΔDII	0	0	100	1.2

The accuracy of the volume fractions calculated with OLIGOMER (Konarev et al., 2003) is about 2% for all constructs.

other. Each hexamer is composed of alternating R1ΔDII and R2ΔDII monomers, as illustrated in Fig. 1a and b. The complex crystallized in space group $C222_1$ with only one heterohexamer in the asymmetric unit. The two heterohexamers in the dodecameric structure are related by a crystallographic 2-fold rotation axis, so that each R1ΔDII and R2ΔDII monomer in one hexamer interacts with one R1ΔDII and one R2ΔDII monomer from the second hexamer. Nucleotide-binding pockets in each heterohexamer are close to the top and bottom faces of the dodecamer, while interactions between the hexameric rings occur through the retained parts of domains II (Fig. 1). This arrangement is further supported by the crystal packing, where the hexamers clearly pack as dodecamers in a head to tail arrangement and do not form staggered layers as was the case for the RuvBL1 hexamer. Furthermore, the dodecamers or double hexamers stack at an angle (Supplementary Fig. S2).

Superposition of the individual R1ΔDII and R2ΔDII monomers using the secondary structure matching algorithm (SSM) (Krissinel and Henrick, 2004) with one of the monomers (chain A) in the RuvBL1 structure (Matias et al., 2006) showed no significant differences, with root-mean-square deviations between the matched C^{α} atoms of 0.6 Å for R1ΔDII and 0.8 Å for R2ΔDII. However, the relative orientation of the monomers in the R1ΔDII/R2ΔDII heterohexamer is slightly different from that in the RuvBL1 homohexamer (Matias et al., 2006). Fig. 1c highlights the similarities of the R1ΔDII and R2ΔDII monomers with the structure of the RuvBL1 monomer. In the following discussion, two regions in domain II will be considered: the external region, truncated in R1ΔDII and R2ΔDII, and the internal region, retained in these two monomers. The internal region is formed by two partially structured α-helices X and Y (Figs. 1c and 2 and S1) and one flexible, non-visible part corresponding to residues 161–179 in R1ΔDII and residues 169–181 in R2ΔDII that bridges the α-helices.

In the RuvBL1 hexameric structure (Matias et al., 2006) many residues from the internal region of domain II were missing from the model due to poor or no electron density suggesting high flexibility. However, the association of two heterohexamers into the dodecameric structure of the R1ΔDII/R2ΔDII complex partially stabilized this region and allowed the modeling of additional residues in both helices X and Y (Fig. 1c).

As illustrated in Fig. 2, each helix X in R1ΔDII and R2ΔDII interacts with an equivalent helix from a symmetry-related monomer of the same type through its C-terminal region, while the N-terminal region interacts with an unmodeled loop from a neighboring non-symmetry-related monomer of the other type. Interactions between the hexamers occur mainly between the unmodeled loops P161-K179 in R1ΔDII with the N-terminal region of helix X in R2ΔDII, stabilizing the dodecamer. A similar interaction that mainly contributes to hexamer stabilization occurs between the unmodeled loop T169-E181 in R2ΔDII and the N-terminal region of helix X in R1ΔDII. Small-angle X-ray scattering studies (see below) support the crystallographic results, confirming that in solution the R1ΔDII/R2ΔDII complex exists almost exclusively as a dodecamer.

The data presented here show that the internal region of domain II may be crucial for the formation of the complex whereas its external region may have other functions, such as interacting with DNA (Matias et al., 2006).

3.2. Nucleotide-binding pocket

Although no ATP was added at any stage during purification or crystallization, the nucleotide-binding pockets of every R1ΔDII and R2ΔDII monomer in the complex clearly show electron density (Fig. 3 and Supplementary Fig. S3) that can be interpreted as a mixture of ADP/Mg^{2+} and ATP. The nucleotide electron density was modeled as ATP in all R1ΔDII and R2ΔDII monomers, but in the final $|F_0| - |F_c|$ electron density map, a large negative peak around the γ-phosphates of the ATP molecules in the R1ΔDII monomers suggested partial ATP hydrolysis. This hypothesis was confirmed by additional structure refinements (data not shown).

The nucleotides are tightly packed in pockets located at the interface between domains I and III (Fig. 1a), as seen in the RuvBL1 structure (Matias et al., 2006). These pockets contain all the conserved motifs typical for AAA^{+} family members, namely Walker A, Walker B, sensor 1 and sensor 2 as represented in Fig. 3 and Supplementary Figs. S1 and S4. Assuming that an ATP molecule is bound in the pocket of R1ΔDII, its γ-phosphate would be stabilized by two hydrogen bonds to Thr 91 and Arg 315, one van der Waals interaction to Asp 213 and one hydrogen bond to Asp 267 from a neighboring R2ΔDII monomer in the hexamer. The ATP γ-phosphate stabilization in the pocket of R2ΔDII is slightly different, featuring two hydrogen bonds to Thr 99 and Asp 214 and one further hydrogen bond to Asp 267 from a neighboring R1ΔDII monomer. The interactions between the γ-phosphate oxygens and the side-chains of Asp residues and between Arg 315 and Mg^{2+} are very likely mediated by water molecules, which cannot be fully resolved at 3 Å resolution.

Normally, the ATPase-activating residue in the nucleotide-binding pocket is an arginine or in some cases a lysine residue (Gai et al., 2004). In the R1ΔDII/R2ΔDII complex, the side-chain of the putative *trans*-finger Arg 268 from a neighboring monomer is pointing away from the pocket. The main difference between the R1ΔDII and R2ΔDII pockets is the position of the *cis* "sensor" finger Arg 315, that in R1ΔDII is in a similar position to the equivalent arginine in RuvBL1, while in R2ΔDII it is oriented away from the pocket.

3.3. Quaternary structure in solution

SAXS was employed to test whether the crystallographic model of R1ΔDII/R2ΔDII corresponds to the oligomeric state in solution. The experimental radius of gyration $R_g = 55 \pm 2$ Å agrees well with the R_g computed from the dodecameric crystal structure of the R1ΔDII/R2ΔDII complex ($R_g = 55$ Å). The low resolution shape of the construct obtained *ab initio* from the scattering data of R1ΔDII/R2ΔDII fits the data with discrepancy $\chi = 1$ (Fig. 4a,

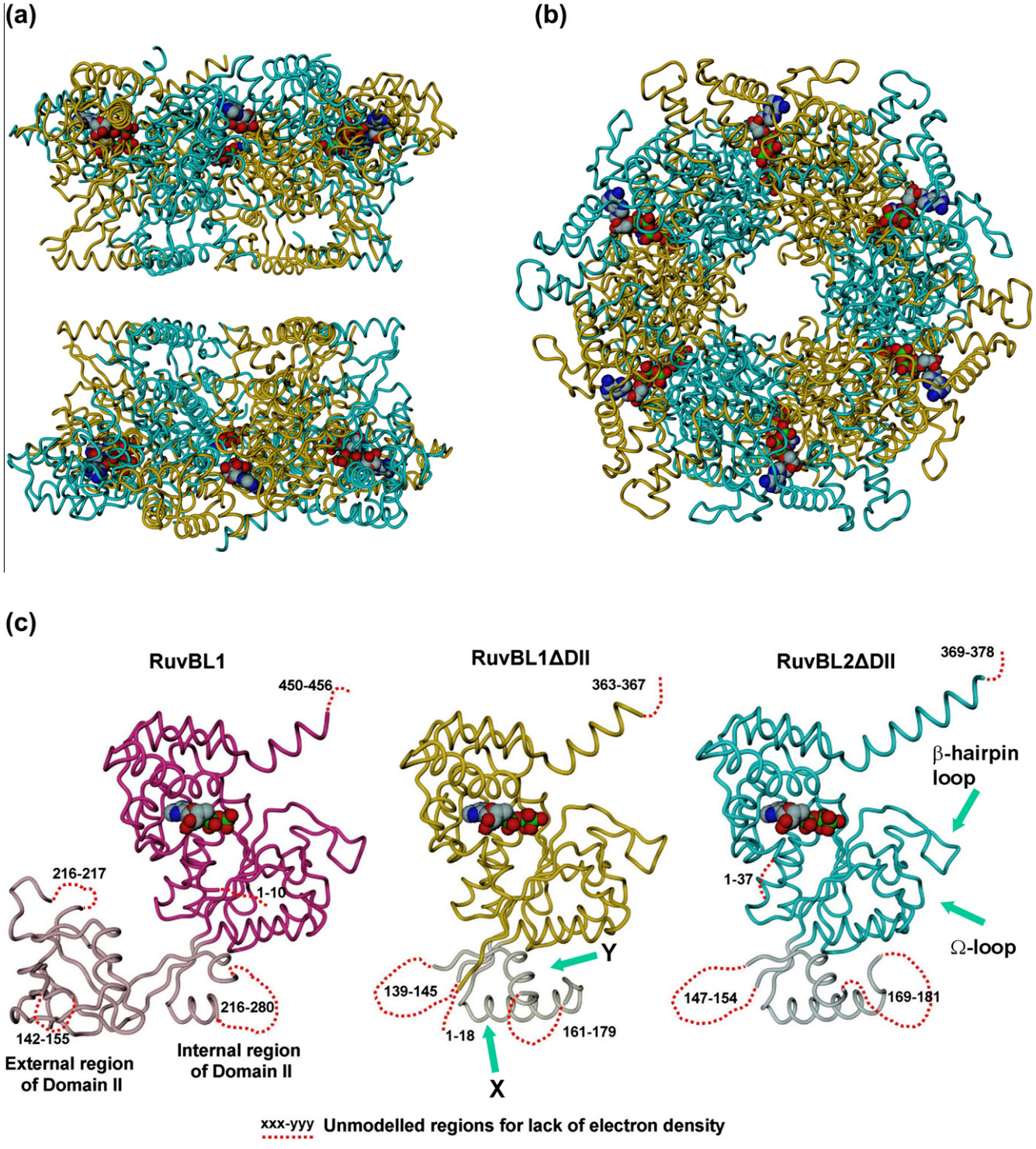

Fig. 1. The R1ΔDII/R2ΔDII complex and comparison of RuvBL1 vs. R1ΔDII and R2ΔDII monomers. (a) Side and (b) top views of the dodecamer. R1ΔDII and R2ΔDII monomers are drawn as tube C^{α} diagrams and are colored gold and cyan, respectively. ATP molecules are drawn as space-filling with atom colors light cyan for carbon, red for oxygen, blue for nitrogen and green for phosphorus. (c) Comparison of the RuvBL1 monomer (whole domain II colored light pink) with the R1ΔDII (retained part of domain II shown in light cyan) and R2ΔDII monomers (retained part of domain II shown in light cyan). R1ΔDII and R2ΔDII were obtained by truncating residues T127-E233 and E134-E237 in their respective wild-type protein chains. Residue numbering refers to the amino acid sequence of the respective protein. Dashed lines represent unmodeled regions for lack of electron density. The external and internal regions of domain II are labeled in the RuvBL1 monomer for clarity. The α-helices X and Y, as well as the β-hairpin and Ω loops mentioned in the text are indicated by arrows in R1ΔDII and R2ΔDII, respectively. Figure prepared with DINO (http://www.dino3d.org).

curve 4) and has an overall appearance similar to the dodecameric crystal structure (Fig. 4b). The experimental R_g exceeds significantly the value computed for the single ring of the crystallographic hexamer of R1ΔDII/R2ΔDII (45 Å) and the scattering pattern evaluated from the hexamer shows a poor fit ($\chi = 25.5$) to the data (Fig. 4b, curve 2). These data clearly demonstrate that in solution, and under the experimental conditions used, the predominant oligomeric form of the R1ΔDII/R2ΔDII complex is a

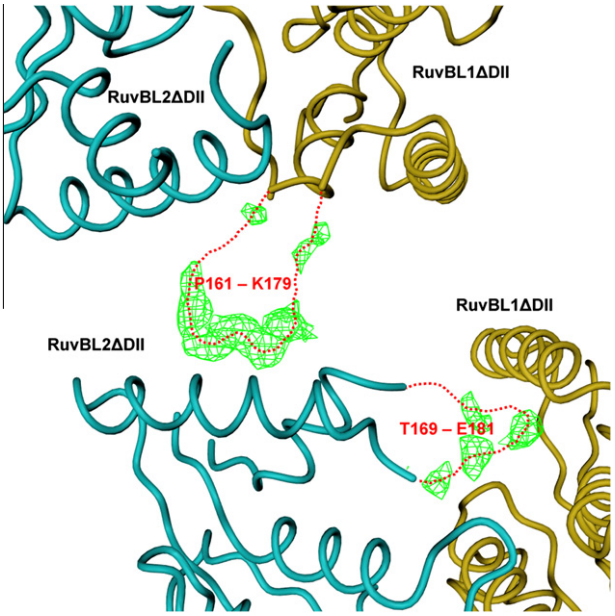

Fig. 2. Interface between the R1ΔDII/R2ΔDII hexamers in the dodecamer. The R1ΔDII and R2ΔDII monomers are colored gold and cyan, respectively. The dotted red lines represent loop regions which could not be modeled due to poor electron density. The final $|F_o| - |F_c|$ electron density in these regions is drawn in green color at the 2.5 σ level. Figure prepared with DINO (http://www.dino3d.org).

dodecamer. Interestingly, and contrary to the results of a recent study (Niewiarowski et al., 2010) which suggested that truncation of DII destabilizes the RuvBL1/RuvBL2 dodecamer formation, the SAXS results indicate that it is the native RuvBL1/RuvBL2 complex that contains a significant fraction of hexamers in solution. This may explain the lack of success in crystallizing the full-length complex.

To further reconcile the observed scattering data with the crystallographic dodecameric assembly, amino acid residues belonging to the unstructured regions missing in this crystal structure were added using the program BUNCH (Petoukhov and Svergun, 2005) with *P*32 symmetry (Fig. 4a, curve 3) yielding a reasonable fit to the experimental data with $\chi = 1.5$, but also displaying some systematic deviation (fit not shown). They reflect the limitations of the missing chains addition, which were performed using P32 symmetry. Allowing for asymmetry in the missing chains using the program CORAL yields an improved fit with $\chi = 1.2$. Most of the added residues (Fig. 4b, shown in blue) were placed in the central cavity, whereby those located around the hexameric rings might reflect slight changes in the overall organization of the dodecamer in the crystal and in solution. Note that the residual systematic deviations in the computed scattering from the dodecamer (Fig. 4a, curve 3) to the experimental data at higher angles ($s > 0.13$ Å^{-1}) occur beyond the resolution range responsible for the overall structure. These results strongly support the dodecameric quaternary structure of the R1ΔDII/R2ΔDII complex observed in the crystal.

A recent paper suggested that histidine-tagged constructs of yeast RuvBL proteins induced the assembly of double hexameric ring RuvBL1/RuvBL2 complexes, while untagged versions of these proteins assembled into single hexameric rings (Cheung et al., 2010). It is worth mentioning that there are important differences between Cheung et al. and our studies. Cheung et al. expressed both yeast Rvb1 and Rvb2 proteins separately as N-terminal His-tagged proteins, while we co-expressed human His-tagged RuvBL1 and FLAG-tagged RuvBL2. Cheung et al. assembled the complex *in vitro* and different oligomeric fractions were separated by a gel filtration column. In our study, the human complex already assembled within the cell by co-expression and was co-purified using three different purification steps (NiNTA, FLAG affinity column and gel filtration).

In the present study the His-tag was not cleaved before crystallization of the human RuvBL complex, but the effect of the His-tag on oligomerization had been assessed by removing it from the RuvBL1 molecules in the complex and analyzing the complex by a gel filtration column. The 6xHis-tag was cleaved using the protease Thrombin during the second purification step when the RuvBL complex was bound to the FLAG beads. The results demonstrate that the 6xHis tag had no influence on the oligomerization state

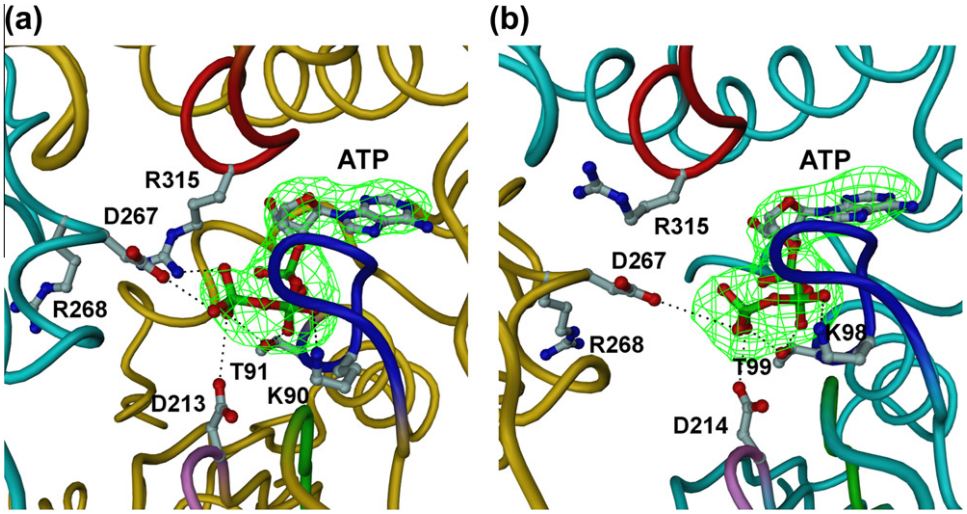

Fig. 3. The nucleotide-binding pocket in the R1ΔDII/R2ΔDII complex. Views of the protein/nucleotide interactions in the R1ΔDII (a) and R2ΔDII (b) nucleotide-binding pockets. The R1ΔDII and R2ΔDII monomers are represented as C^{α} tubes and colored gold and cyan, respectively. In each monomer, the Walker A region is colored blue, the Walker B region is colored violet, the Sensor 1 region is colored green, and the Sensor 2 region is colored red. The ATP molecule and the side-chains of interacting protein residues mentioned in the text are shown in ball-and-stick representation. The atom colors are as in Fig. 1a. Hydrogen bonds between oxygen atoms of the β- and γ-phosphate groups of ATP and protein residue side chains are drawn as black dotted lines. The $|F_o| - |F_c|$ electron density after an initial refinement without ATP in the model is drawn in green color at the 3.0 σ level. A stereo version of this figure is presented in *Supplementary* Fig. S3. Hydrogen bond distances are presented in tables in *Supplementary* Fig. S3. Figure prepared with DINO (http://www.dino3d.org).

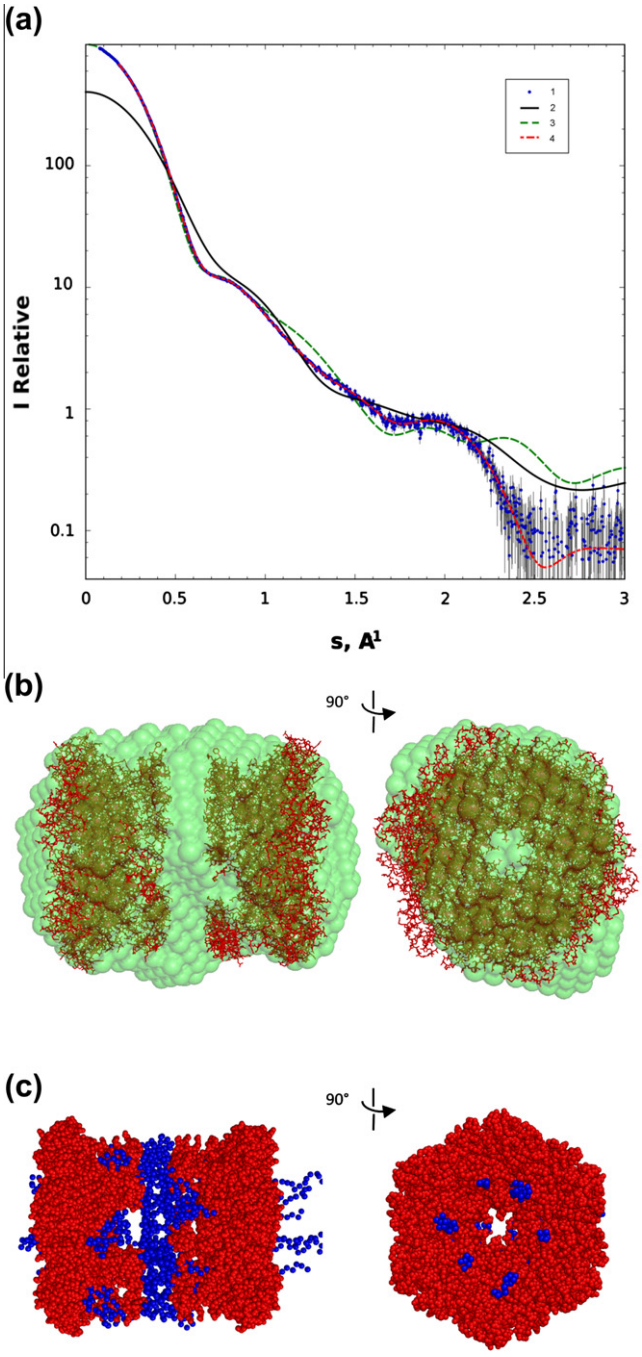

Fig. 4. Scattering and models of RuvBL1ΔDII/RuvBL2ΔDII structure. (a) (1) Composite scattering from RuvBL1ΔDII/RuvBL2ΔDII (blue points) obtained using standard methods from three data sets with concentration 0.9, 11.2 and 21.8 mg/ml. At low angles the composite data are essentially extrapolated to zero solute concentration; (2) fit by the crystallographic hexamer (solid black); (3) fit by the crystallographic dodecamer after addition of missing fragments with P1 symmetry using CORAL (dashed green); (4) fit from the *ab initio* model (dot-dashed red). (b) *Ab-initio* shape of RuvBL1ΔDII/RuvBL2ΔDII (semi-transparent beads), overlaid on the crystal structure (ball-and-stick). (c) CORAL model calculated from the crystallographic model in P32 symmetry (red beads) with added missing amino acids in P1 symmetry (blue beads). In (b) and (c) the right view is rotated counter clockwise by 90° along the vertical axis.

of the human R1ΔDII/R2ΔDII complex under our expression and purification conditions (Supplementary Fig. S4a). After removal of the 6xHis tag, the R1ΔDII/FLAG-R2ΔDII complex elutes at the same position as the 6xHis-R1ΔDII/FLAG-R2ΔDII. The protein standard peaks strongly suggest that the R1ΔDII/R2ΔDII complex elutes from the gel filtration column as a dodecamer (Supplementary Fig. S4b) with an estimated molecular weight of 500 kDa. However, it is important to note that the gel filtration column used did not have the sensitivity and resolution to rule out the presence of a small percentage of hexamers in solution. These results are in agreement with our SAXS data indicating that the dodecameric quaternary structure of the R1ΔDII/R2ΔDII complex observed in the crystal is also present in solution. Neither the 6xHis- nor the FLAG-tags were visible in the electron density maps of our R1ΔDII/R2ΔDII complex crystal structure, and thus were not modeled. However, they are very likely located on the outside of the rings and therefore it is not clear how they could influence oligomerization. Cheung et al. also showed that the His-tag induced dodecamer formation in the yeast Rvb1/Rvb2 complex was reversible, i.e., upon tag removal the dodecamers dissociated into hexamers (Cheung et al., 2010). Since the human 6xHis-R1ΔDII/FLAG-R2ΔDII complex did not dissociate upon His-tag removal, we conclude that dodecameric assembly of the human complex was not His-tag induced.

3.4. Domain II is involved in regulation of ATP hydrolysis and helicase activity

In order to test the ability of the RuvBL1/RuvBL2 complexes to hydrolyze ATP, all mutants with a truncated domain II were tested for ATPase activity and compared with the wild-type constructs. The AAA$^+$ protein large tumor antigen of simian virus 40 (Sullivan and Pipas, 2002), a hexameric helicase essential for viral DNA replication in eukaryotic cells (Borowiec et al., 1990), was used as a positive control. The wild-type RuvBL1/RuvBL2 complex exhibited an approximately three times higher ATPase activity than the individual proteins (Fig. 5a), as previously reported (Gribun et al., 2008; Ikura et al., 2000; Puri et al., 2007; Torreira et al., 2008). Possibly, RuvBL1 can act as a cofactor for RuvBL2 and *vice versa*. Several groups demonstrated that the weak *in vitro* ATPase activity of RuvBL1 and RuvBL2 increased synergistically when the proteins formed a double-hexameric complex showing that this is the enzymatically active form (Ikura et al., 2000; Niewiarowski et al., 2010; Puri et al., 2007). Surprisingly, the single domain II-truncated proteins by themselves (R1ΔDII, R2ΔDII) showed an almost 2-fold activity increase compared to their wild-type counterparts (Fig. 5b). Furthermore, the RuvBL1/RuvBL2 complexes with truncated domains II (RuvBL1/R2ΔDII and R1ΔDII/R2ΔDII) exhibited even higher ATPase activities (Fig. 5b). The activity of individual RuvBL proteins (Matias et al., 2006) and of the complexes was not further stimulated by single- or double-stranded DNA (Fig. 5a), even though Gribun et al. have found that specific DNA substrates stimulated the ATPase activity of the yeast RuvBL proteins (Gribun et al., 2008).

A lack of helicase activity has been reported for purified recombinant RuvBL1 and RuvBL2 (Ikura et al., 2000; Matias et al., 2006; Qiu et al., 1998). Since the DII-truncated mutants of the RuvBL proteins exhibited an unexpected increase in ATPase activity (Fig. 5b), we tested whether higher ATP consumption allowed the exertion of helicase activity. Indeed, such activity was observed with the truncated constructs R1ΔDII, R2ΔDII, RuvBL1/R2ΔDII and R1ΔDII/R2ΔDII (Fig. 5c). Since the wild-type proteins exhibited no helicase activity *in vitro* we conclude that under our assay conditions DNA unwinding by human RuvBL1 and RuvBL2 can be autoinhibited by domain II.

Importantly, the complex of RuvBL1 and RuvBL2 with truncated domains II was dodecameric in solution at all concentrations measured, as examined in SAXS experiments. This result indicates that the oligomeric state in the helicase assay most likely corresponds to the dodecameric state in the crystal structure. Even though the protein concentration used in the helicase assay was very

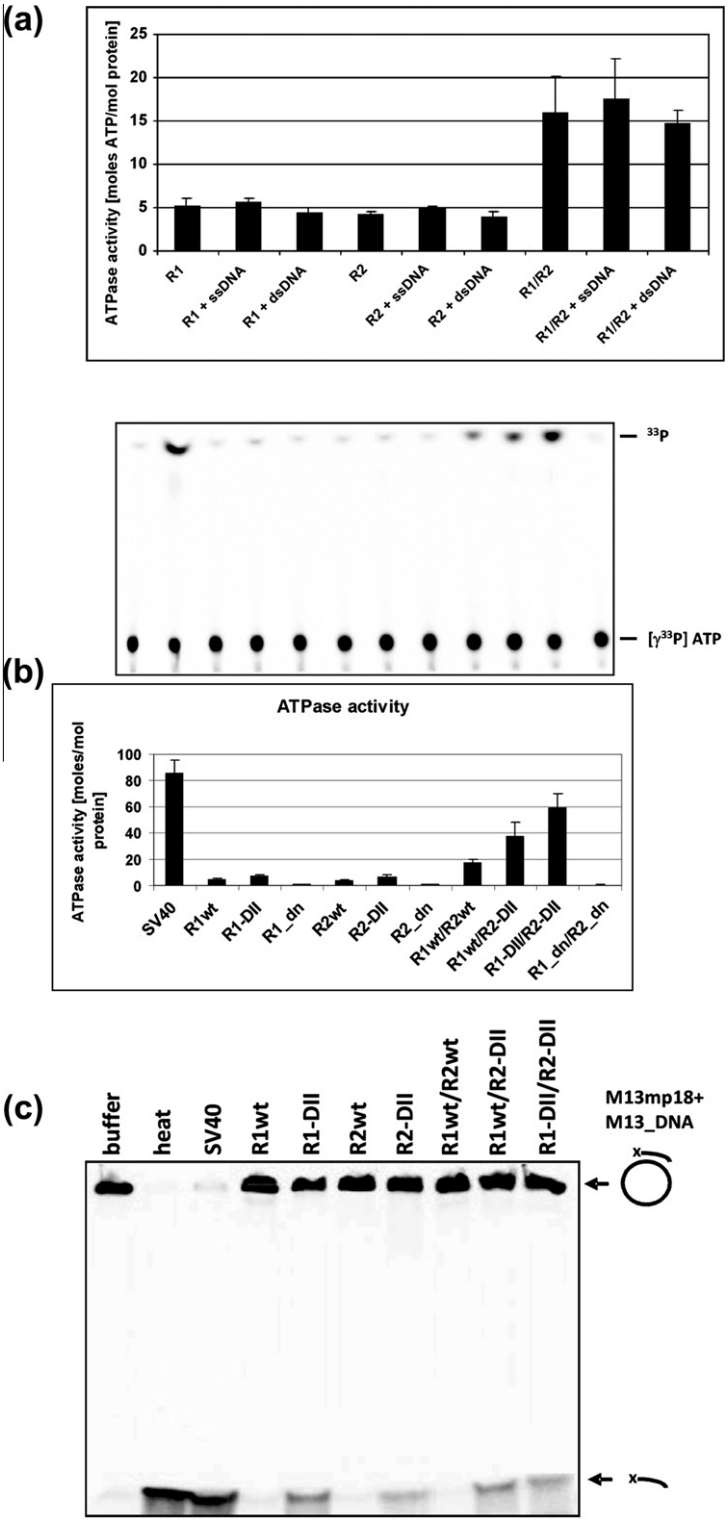

Fig. 5. ATPase and helicase activity studies of the RuvBL1, RuvBL2 and RuvBL1/RuvBL2 complexes. (a) ATPase activity of both the individual monomers and the complex was tested in the presence and absence of single and double-stranded DNA. The ATPase activity of the RuvBL1/RuvBL2 complex increased 3-fold in comparison with that of the isolated RuvBL1 and RuvBL2. *In vitro* ATPase activity was not affected by the presence of ss or dsDNA. (b) ATPase activity of wild-type and truncated versions of RuvBL1 and RuvBL2 monomers and RuvBL1/RuvBL2 complexes; SV40 LTag helicase was used as positive control. The activity of the wild-type RuvBL1/RuvBL2 complex (R1wt/R2wt) hydrolyzing 17 mol of ATP per mole of protein in 30 min, increased to 37 mol of ATP in the complex composed of wild-type RuvBL1 and truncated RuvBL2 (R1wt/R2ΔDII). The truncated complex (R1ΔDII/R2ΔDII) was even more active, hydrolyzing 60 mol of ATP, representing 70% of SV40 Ltag's activity. (c) Helicase activity was not detected for the wild-type proteins. In contrast, all proteins with truncated domains II were shown to exhibit *in vitro* helicase activity. SV40 LTag helicase protein was used as positive control.

low and not tested in analytical gel filtration experiments, this and previous studies have shown that the double-hexameric complex exhibits the highest ATPase activity (Ikura et al., 2000; Niewiarowski et al., 2010; Puri et al., 2007). Therefore, we assume that we solved the crystal structure of a biologically active dodecameric RuvBL1/RuvBL2 complex competent for helicase activity.

3.5. The central channel of the dodecamer exhibits characteristics for interaction with single-stranded nucleic acids

The central channel of the dodecamer is approximately 85 Å long and its internal diameter (measured between C^{α} atoms) ranges between 17 and 21 Å (Supplementary Fig. S5) at either end, while it is much wider in the central part (33–38 Å). At both ends of the channel, each monomer displays a β-hairpin structure similar to that found in SV40 LTag (Gai et al., 2004), comprising residues G245-P258 in R1ΔDII and G246-P258 in R2ΔDII whereas in the central section there are Ω-loops formed by residues V115-K122 in R1ΔDII and I123-K130 in R2ΔDII (Fig. 1c). In each hexamer, adjacent monomers interact so that the β-hairpin from one R1ΔDII monomer lies above the Ω-loop from a R2ΔDII monomer, and *vice versa*. These secondary structure motifs in the R1ΔDII/R2ΔDII complex are similarly positioned as in the RuvBL1 hexamer (Matias et al., 2006). Interactions with nucleic acids mediated by one or more loops in the central channels of AAA^{+} proteins have been observed for ssDNA- and dsDNA-binding members of this family. However, the alternation of charges in the central channel of the dodecamer shown in Supplementary Fig. S6, combined with the diameter of the channel suggests interactions with single-stranded nucleic acids. Single-stranded DNA-binding to the full-length RuvBL1/RuvBL2 complex was tested using an electrophoretic mobility shift assay (Supplementary Fig. S7). Indeed, the complex bound to ssDNA, but binding was significantly weaker than that observed with purified RuvBL1 (Matias et al., 2006). Since domain II constitutes the interaction site in the RuvBL complex between the two hexameric rings to form the dodecamer, it may not be completely available for DNA-binding of the RuvBL1/RuvBL2 complex. Therefore, it is conceivable that the demonstrated ssDNA-binding shown in Supplementary Fig. S7 occurs in part through the central channel of the RuvBL1/RuvBL2 complex.

4. Discussion

In this work, we have solved the first crystal structure of the biologically active RuvBL1/RuvBL2 complex at 3 Å resolution, which is a double hexameric ring composed of alternating RuvBL1 and RuvBL2 monomers. The dodecameric assembly observed in the crystal is supported by the crystal packing and SAXS results in solution. Unfortunately, the protein regions responsible for the interactions between two hexameric rings could not be modeled due to poor electron density. This can be rationalized by noting that a crystal structure is always a time and space average of its constituent molecules. Often, certain regions in a molecule will occupy different places in adjacent unit cells. This results in a blurred electron density and can prevent model building of that region in the molecule. This is very likely the case with the complex crystal structure reported herein. As already noted, the ATP present in the RuvBL1 monomers seems to be partially hydrolyzed to ADP, a hint that the complex was not crystallized in a conformationally uniform state. If structural changes are internal to the dodecamer they will not necessarily affect the crystal packing. Due to the averaging effect of the crystal structure no clear electron density will be visible, even though interactions between the hexameric rings are indeed present. These considerations might also explain the low diffraction quality observed for the RuvBL1/RuvBL2 complex crystals.

The presented results underline the importance of the joint use of solution scattering together with crystallographic analysis for macromolecular complexes. The crystallographic studies providing high resolution structures are meaningfully complemented by SAXS characterizing low resolution structures and oligomeric behavior of a much broader palette of complexes independently of their ability to be crystallized. Importantly and in contrast to other methods for characterization of oligomeric compositions, SAXS allows the monitoring of concentration-dependent effects and provides information about the quaternary structure and oligomeric content.

The three-dimensional structure of the RuvBL1/RuvBL2 complex, combined with the results of the biochemical studies presented in this work, demonstrates that the structural organization of these highly conserved proteins is typical for helicase members of the AAA^{+} family and that the complex possesses all the features characteristic of molecular machines. ATPases of the AAA^{+} family, which include RuvBL1 and RuvBL2, convert chemical energy from ATP hydrolysis into mechanical motion that can be used for a variety of functions such as dsDNA unwinding. The wild-type RuvBL1/RuvBL2 complex exhibits a 3- to 4-fold increase in ATP consumption compared to the single proteins, and the truncated dodecameric complex shows a further 3-fold increase in ATP consumption. These data combined with our structural analyses suggest that a stable assembly of RuvBL1 and RuvBL2 into a dodecameric structure stimulates ATPase activity. Although the details of activation are not evident from the present crystal structure, this synergistic effect on enzymatic activity clearly suggests strong communication between both proteins, in agreement with previous work (Ikura et al., 2000; Niewiarowski et al., 2010; Puri et al., 2007).

Diverse examples support the notion that ATPase consumption by RuvBL1 and RuvBL2 is activated when they are part of multiprotein complexes. The p400 complex participates in chromatin remodeling events and displays ATPase and helicase activities, which are at least in part contributed by RuvBL1 and RuvBL2 (Fuchs et al., 2001). In addition, it has been shown that the ATPase activity of RuvBL1 is needed for the chromatin remodeling function of the TIP60 complex in order to allow transcription of TCF-dependent cellular genes, such as ITF-2. The Walker B mutant RuvBL1_D302N inhibits ITF-2 gene expression, which is linked to decreased acetylation of histones in the vicinity of the TCF-binding sites in the ITF-2 promoter region (Feng et al., 2003). These findings not only suggest that the ATPase activity of RuvBL1 is important for β-catenin/TCF gene regulation, but are also compatible with a direct role of RuvBL1 in chromatin remodeling.

Helicases known to bind ssDNA have channel sizes similar to that in the dodecameric structure of R1ΔDII/R2ΔDII (Enemark and Joshua-Tor, 2006; Singleton et al., 2000). In addition, the charge distribution of the channel formed at the center of the RuvBL1/RuvBL2 complex (Supplementary Fig. S7) suggests accommodation of ssDNA. Since helicase activities of RuvBL1 and RuvBL2 are still a matter of debate, we tested such activity using the highly purified proteins. These experiments showed that RuvBL1 and RuvBL2 individually or in complex can process DNA *in vitro* only when their domain II is truncated, in agreement with previous results where no activity was detected for the wild-type proteins (Ikura et al., 2000; Qiu et al., 1998). These data suggest that DNA helicase activity of human RuvBL1 and RuvBL2 can be autoinhibited by domain II. *In vivo* cofactors within chromatin remodeling complexes might bind to RuvBL1 and RuvBL2, altering the conformation of domain II and allowing them to exert their helicase activity. This process would be similar to that observed for the bacterial homolog RuvB which has weak ATPase and helicase activities *in vitro* and requires RuvA as a partner for its *in vitro* and *in vivo* activities (Putnam et al., 2001). Importantly, the bacterial helicase RuvB does not contain the 174 residue insertion (Matias et al., 2006), which forms domain II of RuvBL1 and RuvBL2. Since helicase activity was only detected using the RuvBL1 and RuvBL2 constructs with a truncated domain II, we conclude that domain II is not needed for this activity and may have regulatory functions *in vivo*. However, helicase activity studies of the RuvBL proteins

were performed by different groups and have been controversial. A 3′-to-5′ helicase activity was found for rat RuvBL1 (Makino et al., 1999), while RuvBL2 exhibited a 5′-to-3′ activity (Kanemaki et al., 1999). In addition, Gribun et al. showed that the heterohexameric yeast RuvBL1/RuvBL2 complex possesses helicase activity (Gribun et al., 2008). On the other hand, a lack of helicase activity has been reported for purified recombinant RuvBL1 and RuvBL2 (Ikura et al., 2000; Matias et al., 2006; Qiu et al., 1998). Therefore, future experiments will be necessary to clarify the existing controversial helicase activity data.

Previous findings demonstrated that RuvBL1 and RuvBL2 can act as essential molecular chaperones in processes where no helicase activity is needed, for example in assembling the multi-subunit INO80 chromatin remodeling complex. Jonsson et al. showed that both RuvBL proteins bound to ATP are in the correct conformation to assemble the functional INO80 complex without the need of ATPase and helicase activities (Jonsson et al., 2004). In addition, Jonsson et al. presented that the RuvBL proteins are functional parts of the INO80 chromatin remodeling complex as double hexamers (Jonsson et al., 2004). These data further support the conclusion that we crystallized a biologically relevant dodecameric complex and are also in agreement with the 1:6:6 stoichiometry of INO80 to RuvBL1 and RuvBL2 in the INO80 complex published by Shen et al. (2000).

Furthermore, our SAXS results show that in solution the R1ΔDII/R2ΔDII dodecameric complex is far more stable than the wild-type RuvBL1/RuvBL2 complex. The latter is in equilibrium with a significant fraction of hexamers indicating that truncation of the flexible domain II favors the dodecameric assembly. However, the flexibility between the hexameric rings might be an important regulatory feature of the complex *in vivo*. Since RuvBL1 and RuvBL2 are involved in diverse cellular functions, it is conceivable that different functional RuvBL1/RuvBL2 complexes exist within the cell. The overall assembly observed in the RuvBL1/RuvBL2 crystal structure could also be modified by association with external cofactors that might be important for "*in vivo*" activation of the helicase activity.

High resolution crystal structures of the SV40 Ltag helicase were reported in three distinct nucleotide-binding states, where all active sites are either empty or complexed with ATP or ADP (Gai et al., 2004). These results clearly suggest an all-or-none nucleotide-binding mode and a concerted ATP hydrolysis mechanism. The R1ΔDII/R2ΔDII dodecameric complex structure seems to be trapped in an intermediate state of the ATP hydrolysis reaction, showing a mixture of ATP/ADP molecules bound to the R1ΔDII monomers in the heterohexamers. Given that all nucleotide-binding pockets are occupied, it is conceivable that RuvBL1/RuvBL2 also uses the concerted mode for ATP hydrolysis, which is different from the sequential mechanism for other known hexameric machines (Leslie et al., 1999; Singleton et al., 2000; Stock et al., 1999).

A recent study raised concerns that using His-tagged constructs may influence the oligomerization states of RuvBL1/RuvBL2 complexes (Cheung et al., 2010). However, in this work a different tag approach was used, a combination of 6xHis and FLAG tags. The oligomerization state of this complex was not affected by the presence of a His-tag as shown by gel filtration experiments before and after removal of the tag. Importantly, the dodecameric R1ΔDII/R2ΔDII complex was shown to be active, probably mimicking an *in vivo* conformation that can only be attained in the presence of regulatory cofactors.

Interestingly, the crystal structure reported herein differs from the previously reported structural results based on EM studies in several important aspects. Firstly, the dodecamer is symmetrical in contrast to the EM structures proposed by Puri et al. (2007) and Torreira et al. (2008). Secondly, the heterohexameric arrangement of R1ΔDII and R2ΔDII monomers agrees with that proposed by Gribun et al. (2008) although the complex structure is clearly a dodecamer while they proposed isolated hexamers. In addition and in agreement with the present results, the dodecameric yeast Rvb1/Rvb2 cryo-EM structure reported by Torreira et al. (2008) clearly shows that domain II constitutes the interaction site between the two hexameric rings. However, Torreira et al. suggests that each ring is composed of just one of the proteins, forming homo-oligomeric hexamers. Nevertheless, it should be considered that the RuvBL1 and RuvBL2 structures are very similar, and that despite the fact that more than one hundred crystals were screened, the best resolution obtained from native R1ΔDII/R2ΔDII crystals barely reached 4 Å (Gorynia et al., 2008). Although the structure could be solved by molecular replacement, a clear distinction between R1ΔDII and R2ΔDII monomers was not possible, and a Selenomethionine derivative crystal which diffracted to 3 Å resolution was required to elucidate the composition of the complex. Consequently, the asymmetric hexamer shape reported by Torreira et al. (Torreira et al., 2008) should be regarded with some caution, as it may correspond to different conformational states of the RuvBL1 and RuvBL2 monomers in each hexamer rather than an indication that the dodecamer is composed of two homohexamers, one of RuvBL1 monomers and the other of RuvBL2 monomers. It is intriguing that different EM structures for the RuvBL1/RuvBL2 complex exist, and that none agree with the first determined crystal structure of this complex. However, it should be noted that in each case different complex preparation methods were employed: coexpression of human His-RuvBL1/FLAG-RuvBL2 in *E.coli* (this work), coexpression of yeast RuvBL1/His-RuvBL2 in insect cells (Torreira et al., 2008), separately expressed yeast His-RuvBL1 and His-RuvBL2 in *E. coli* (Gribun et al., 2008), and separately expressed human His-RuvBL1 and RuvBL2-His in *E. coli* (Puri et al., 2007). Given that RuvBL1 and RuvBL2 are essential components of several important complexes, it is very likely that the cellular activities of these proteins are regulated by cofactors. It is possible that different forms of the RuvBL1/RuvBL2 complex exist *in vivo*, hexameric or dodecameric, tailored by external cofactors according to the different functions they perform. It will be an exciting challenge for the future to identify these cofactors and determine the structures of the complexes that they form with RuvBL1 or RuvBL2. Knowledge of how the function of RuvBL1 and RuvBL2 is regulated by the different steps of ATP hydrolysis and by interacting proteins will deepen our understanding of the essential role RuvBL1 and RuvBL2 play in biological processes.

Acknowledgments

We thank Peter Lindley, Bernard Haendler (Bayer Schering Pharma) and Carlos Frazão (ITQB-UNL) for helpful suggestions, discussions and comments on the manuscript. This work was supported by European Commission funding through the SPINE2-COMPLEXES project LSHG-CT-2006-031220. ESRF support for the ID-29 data collection and EU support for the SAXS measurements at X33 (FP7/2007-2013 under Grant agreement No. 226716) are also acknowledged.

Appendix A. Supplementary data

Supplementary data associated with this article can be found, in the online version, at doi:10.1016/j.jsb.2011.09.001.

References

Abrahams, J.P., Leslie, A.G.W., 1996. Methods used in the structure determination of bovine mitochondrial F1 ATPase. Acta Crystallogr. D Biol. Crystallogr. 52, 30–42.

Adams, P.D., Grosse-Kunstleve, R.W., Hung, L.W., Ioerger, T.R., McCoy, A.J., et al., 2002. PHENIX: building new software for automated crystallographic structure determination. Acta Crystallogr. D Biol. Crystallogr. 58, 1948–1954.

Bauer, A., Huber, O., Kemler, R., 1998. Pontin52, an interaction partner of beta-catenin, binds to the TATA box binding protein. Proc. Natl. Acad. Sci. USA 95, 14787–14792.

Bauer, A., Chauvet, S., Huber, O., Usseglio, F., Rothbacher, U., et al., 2000. Pontin52 and reptin52 function as antagonistic regulators of beta-catenin signalling activity. EMBO J. 19, 6121–6130.

Berman, H.M., Westbrook, J., Feng, Z., Gilliland, G., Bhat, T.N., et al., 2000. The Protein Data Bank. Nucleic Acids Res. 28, 235–242.

Blanc, J.F., Lalanne, C., Plomion, C., Schmitter, J.M., Bathany, K., et al., 2005. Proteomic analysis of differentially expressed proteins in hepatocellular carcinoma developed in patients with chronic viral hepatitis C. Proteomics 5, 3778–3789.

Blow, D.M., 2002. Rearrangement of Cruickshank's formulae for the diffraction-component precision index. Acta Crystallogr. D Biol. Crystallogr. 58, 792–797.

Borowiec, J.A., Dean, F.B., Bullock, P.A., Hurwitz, J., 1990. Binding and unwinding – how T antigen engages the SV40 origin of DNA replication. Cell 60, 181–184.

Bricogne, G., Blanc, E., Brandl, M., Flensburg, C., Keller, P., et al., 2010. BUSTER version 2.9. Global Phasing Ltd., Cambridge, UK.

Brünger, A.T., 1992. Free R value: a novel statistical quantity for assessing the accuracy of crystal structures. Nature 355, 472–474.

Cheung, K.L., Huen, J., Kakihara, Y., Houry, W.A., Ortega, J., 2010. Alternative oligomeric states of the yeast Rvb1/Rvb2 complex induced by histidine tags. J. Mol. Biol. 404, 478–492.

Cole, M.D., 1986. The myc oncogene: its role in transformation and differentiation. Annu. Rev. Genet. 20, 361–384.

Collaborative Computational Project Number 4, 1994. The CCP4 suite: programs for protein crystallography. Acta Crystallogr. D Biol. Crystallogr. 50, 760–763.

Cowtan, K., 1994. 'dm': An automated procedure for phase improvement by density modification. Joint CCP4 and ESF-EACMB Newsletter on Protein Crystallography, Vol. 31. Daresbury Laboratory, Warrington, UK, pp. 34–38.

Cowtan, K., 2006. The Buccaneer software for automated model building. 1. Tracing protein chains. Acta Crystallogr. D Biol. Crystallogr. 62, 1002–1011.

Dehan, E., Ben-Dor, A., Liao, W., Lipson, D., Frimer, H., et al., 2007. Chromosomal aberrations and gene expression profiles in non-small cell lung cancer. Lung cancer 56, 175–184.

Diederichs, K., Karplus, P.A., 1997. Improved R-factors for diffraction data analysis in macromolecular crystallography. Nat. Struct. Biol. 4, 269–275.

Dugan, K.A., Wood, M.A., Cole, M.D., 2002. TIP49, but not TRRAP, modulates c-Myc and E2F1 dependent apoptosis. Oncogene 21, 5835–5843.

Emsley, P., Cowtan, K., 2004. Coot: model-building tools for molecular graphics. Acta Crystallogr. D Biol. Crystallogr. 60, 2126–2132.

Enemark, E.J., Joshua-Tor, L., 2006. Mechanism of DNA translocation in a replicative hexameric helicase. Nature 442, 270–275.

Evans, G., Pettifer, R., 2001. CHOOCH: a program for deriving anomalous-scattering factors from X-ray fluorescence spectra. J. Appl. Crystallogr. 34, 82–86.

Feng, Y., Lee, N., Fearon, E.R., 2003. TIP49 regulates beta-catenin-mediated neoplastic transformation and T-cell factor target gene induction via effects on chromatin remodeling. Cancer Res. 63, 8726–8734.

Fuchs, M., Gerber, J., Drapkin, R., Sif, S., Ikura, T., et al., 2001. The p400 complex is an essential E1A transformation target. Cell 106, 297–307.

Gai, D., Zhao, R., Li, D., Finkielstein, C.V., Chen, X.S., 2004. Mechanisms of conformational change for a replicative hexameric helicase of SV40 large tumor antigen. Cell 119, 47–60.

Gorynia, S., Matias, P.M., Bandeiras, T.M., Donner, P., Carrondo, M.A., 2008. Cloning, expression, purification, crystallization and preliminary X-ray analysis of the human RuvBL1–RuvBL2 complex. Acta Crystallogr. F Struct. Biol. Cryst. Commun. 64, 840–846.

Gribun, A., Cheung, K.L., Huen, J., Ortega, J., Houry, W.A., 2008. Yeast Rvb1 and Rvb2 are ATP-dependent DNA helicases that form a heterohexameric complex. J. Mol. Biol. 376, 1320–1333.

Guinier, A., 1939. La Diffraction des Rayons X aux Très Faibles Angles: Applications à l'Etude des Phénomènes Ultra-microscopiques. Ann. Phys. (Paris) 12, 161–236.

Huber, O., Ménard, L., Haurie, V., Nicou, A., Taras, D., et al., 2008. Pontin and reptin, two related ATPases with multiple roles in cancer. Cancer Res. 68, 6873–6876.

Ikura, T., Ogryzko, V.V., Grigoriev, M., Groisman, R., Wang, J., et al., 2000. Involvement of the TIP60 histone acetylase complex in DNA repair and apoptosis. Cell 102, 463–473.

Jha, S., Dutta, A., 2009. RVB1/RVB2: running rings around molecular biology. Mol. Cell 34, 521–533.

Jonsson, Z.O., Dhar, S.K., Narlikar, G.J., Auty, R., Wagle, N., et al., 2001. Rvb1p and Rvb2p are essential components of a chromatin remodeling complex that regulates transcription of over 5% of yeast genes. J. Biol. Chem. 276, 16279–16288.

Jonsson, Z.O., Jha, S., Wohlschlegel, J.A., Dutta, A., 2004. Rvb1p/Rvb2p recruit Arp5p and assemble a functional Ino80 chromatin remodeling complex. Mol. Cell 16, 465–477.

Kabsch, W., 1993. Automatic processing of rotation diffraction data from crystals of initially unknown symmetry and cell constants. J. Appl. Crystallogr. 26, 795–800.

Kanemaki, M., Kurokawa, Y., Matsu-ura, T., Makino, Y., Masani, A., et al., 1999. TIP49b, a new RuvB-like DNA helicase, is included in a complex together with another RuvB-like DNA helicase, TIP49a. J. Biol. Chem. 274, 22437–22444.

Konarev, P.V., Volkov, V.V., Sokolova, A.V., Koch, M.H.J., Svergun, D.I., 2003. PRIMUS: a Windows PC-based system for small-angle scattering data analysis. J. Appl. Crystallogr. 36, 1277–1282.

Krissinel, E., Henrick, K., 2004. Secondary-structure matching (SSM), a new tool for fast protein alignment in three dimensions. Acta Crystallogr. D Biol. Crystallogr. 60, 2256–2268.

Kusch, T., Florens, L., Macdonald, W.H., Swanson, S.K., Glaser, R.L., et al., 2004. Acetylation by Tip60 is required for selective histone variant exchange at DNA lesions. Science 306, 2084–2087.

Laskowski, R.A., MacArthur, M.W., Moss, D.S., Thornton, J.M., 1993. PROCHECK – a program to check the stereochemical quality of proteins. J. Appl. Crystallogr. 26, 283–291.

Lauscher, J.C., Loddenkemper, C., Kosel, L., Grone, J., Buhr, H.J., et al., 2007. Increased pontin expression in human colorectal cancer tissue. Hum. Pathol. 38, 978–985.

Leslie, A.G., Abrahams, J.P., Braig, K., Lutter, R., Menz, R.I., et al., 1999. The structure of bovine mitochondrial F1-ATPase: an example of rotary catalysis. Biochem. Soc. Trans. 27, 37–42.

Makino, Y., Kanemaki, M., Kurokawa, Y., Koji, T., Tamura, T., 1999. A rat RuvB-like protein, TIP49a, is a germ cell-enriched novel DNA helicase. J. Biol. Chem. 274, 15329–15335.

Matias, P.M., Gorynia, S., Donner, P., Carrondo, M.A., 2006. Crystal structure of the human AAA+ protein RuvBL1. J. Biol. Chem. 281, 38918–38929.

Matthews, B.W., 1968. Solvent content of protein crystals. J. Mol. Biol. 33, 491–497.

Mizuguchi, G., Shen, X., Landry, J., Wu, W.H., Sen, S., et al., 2004. ATP-driven exchange of histone H2AZ variant catalyzed by SWR1 chromatin remodeling complex. Science 303, 343–348.

Morrison, A.J., Shen, X., 2009. Chromatin remodelling beyond transcription: the INO80 and SWR1 complexes. Nat. Rev. Mol. Cell Biol. 10, 373–384.

Murshudov, G.N., Vagin, A.A., Dodson, E.J., 1997. Refinement of macromolecular structures by the maximum-likelihood method. Acta Crystallogr. D Biol. Crystallogr. 53, 240–255.

Neuwald, A.F., Aravind, L., Spouge, J.L., Koonin, E.V., 1999. AAA+: a class of chaperone-like ATPases associated with the assembly, operation, and disassembly of protein complexes. Genome Res. 9, 27–43.

Niewiarowski, A., Bradley, A.S., Gor, J., McKay, A.R., Perkins, S.J., et al., 2010. Oligomeric assembly and interactions within the human RuvB-like RuvBL1 and RuvBL2 complexes. Biochem. J. 429, 113–125.

Petoukhov, M.V., Svergun, D.I., 2005. Global rigid body modeling of macromolecular complexes against small-angle scattering data. Biophys. J. 89, 1237–1250.

Petoukhov, M.V., Konarev, P.V., Kikhney, A.G., Svergun, D.I., 2007. ATSAS 2.1 – towards automated and web-supported small-angle scattering data analysis. J. Appl. Crystallogr. 40, s223–s228.

Porod, G., 1982. General Theory, in: Small-angle X-ray scattering. Academic Press, London, pp. 17–51.

Puri, T., Wendler, P., Sigala, B., Saibil, H., Tsaneva, I.R., 2007. Dodecameric structure and ATPase activity of the human TIP48/TIP49 complex. J. Mol. Biol. 366, 179–192.

Putnam, C.D., Clancy, S.B., Tsuruta, H., Gonzalez, S., Wetmur, J.G., et al., 2001. Structure and mechanism of the RuvB Holliday junction branch migration motor. J. Mol. Biol. 311, 297–310.

Qiu, X.B., Lin, Y.L., Thome, K.C., Pian, P., Schlegel, B.P., et al., 1998. An eukaryotic RuvB-like protein (RUVBL1) essential for growth. J. Biol. Chem. 273, 27786–27793.

Ramachandran, G.N., Sasisekharan, V., 1968. Conformation of polypeptides and proteins. Adv. Protein Chem. 23, 283–438.

Roessle, M.W., Klaering, R., Ristau, U., Robrahn, B., Jahn, D., et al., 2007. Upgrade of the small-angle X-ray scattering beamline X33 at the European Molecular Biology Laboratory, Hamburg. J. Appl. Crystallogr. 40, s190–s194.

Rousseau, B., Ménard, L., Haurie, V., Taras, D., Blanc, J.F., et al., 2007. Overexpression and role of the ATPase and putative DNA helicase RuvB-like 2 in human hepatocellular carcinoma. Hepatology 46, 1108–1118.

Samuelson, A.V., Narita, M., Chan, H.M., Jin, J., de Stanchina, E., et al., 2005. P400 is required for E1A to promote apoptosis. J. Biol. Chem. 280, 21915–21923.

Shen, X., Mizuguchi, G., Hamiche, A., Wu, C., 2000. A chromatin remodelling complex involved in transcription and DNA processing. Nature 406, 541–544.

Singleton, M.R., Sawaya, M.R., Ellenberger, T., Wigley, D.B., 2000. Crystal structure of T7 gene 4 ring helicase indicates a mechanism for sequential hydrolysis of nucleotides. Cell 101, 589–600.

Smart, O.S., Brandl, M., Flensburg, C., Keller, P., Paciorek, W., et al., 2008. Refinement with Local Structure Similarity Restraints (LSSR) Enables Exploitation of Information from Related Structures and Facilitates use of NCS. Annu. Meet. Am. Crystallogr. Assoc, Knoxville, TN, p. 117.

Stock, D., Leslie, A.G., Walker, J.E., 1999. Molecular architecture of the rotary motor in ATP synthase. Science 286, 1700–1705.

Storoni, L.C., McCoy, A.J., Read, R.J., 2004. Likelihood-enhanced fast rotation functions. Acta Crystallogr. D Biol. Crystallogr. 60, 432–438.

Sullivan, C.S., Pipas, J.M., 2002. T antigens of simian virus 40: molecular chaperones for viral replication and tumorigenesis. Microbiol. Mol. Biol. Rev. 66, 179–202.

Svergun, D., 1992. Determination of the regularization parameter in indirect-transform methods using perceptual criteria. J. Appl. Crystallogr. 25, 495–503.

Svergun, D.I., 1999. Restoring low resolution structure of biological macromolecules from solution scattering using simulated annealing. Biophys. J. 76, 2879–2886.

Svergun, D., Barberato, C., Koch, M.H.J., 1995. CRYSOL – a program to evaluate X-ray solution scattering of biological macromolecules from atomic coordinates. J. Appl. Crystallogr. 28, 768–773.

Torreira, E., Jha, S., Lopez-Blanco, J.R., Arias-Palomo, E., Chacon, P., et al., 2008. Architecture of the pontin/reptin complex, essential in the assembly of several macromolecular complexes. Structure 16, 1511–1520.

Vonrhein, C., Blanc, E., Roversi, P., Bricogne, G., 2007. Automated Structure Solution With autoSHARP. In: Doublié, S. (Ed.), Macromolecular Crystallography Protocols. Humana Press, Totowa, NJ, pp. 215–230.

Walker, J.E., Saraste, M., Runswick, M.J., Gay, N.J., 1982. Distantly related sequences in the alpha- and beta-subunits of ATP synthase, myosin, kinases and other ATP-requiring enzymes and a common nucleotide binding fold. EMBO J. 1, 945–951.

Wood, M.A., McMahon, S.B., Cole, M.D., 2000. An ATPase/helicase complex is an essential cofactor for oncogenic transformation by c-Myc. Mol. Cell 5, 321–330.

Yamada, K., Kunishima, N., Mayanagi, K., Ohnishi, T., Nishino, T., et al., 2001. Crystal structure of the Holliday junction migration motor protein RuvB from *Thermus thermophilus* HB8. Proc. Natl. Acad. Sci. USA 98, 1442–1447.